

# Giant magnetoresistance induced by spin-dependent orbital coupling in Fe<sub>3</sub>GeTe<sub>2</sub>/graphene heterostructures

Received: 6 September 2024

Accepted: 14 March 2025

Published online: 24 March 2025

 Check for updatesShiming Huang<sup>1</sup>, Lianying Zhu<sup>1</sup>, Yongxin Zhao<sup>1</sup>, Kenji Watanabe<sup>2</sup>, Takashi Taniguchi<sup>2</sup>, Jie Xiao<sup>3</sup>, Le Wang<sup>4</sup>, Jiawei Mei<sup>3</sup>, Huolin Huang<sup>5</sup>, Feng Zhang<sup>1</sup>✉, Maoyuan Wang<sup>1</sup>✉, Deyi Fu<sup>1</sup>✉ & Rong Zhang<sup>1</sup>

Information technology has a great demand for magnetoresistance (MR) sensors with high sensitivity and wide-temperature-range operation. It is well known that space charge inhomogeneity in graphene (Gr) leads to finite MR in its pristine form, and can be enhanced by increasing the degree of spatial disorder. However, the enhanced MR usually diminishes drastically as the temperature decreases. Here, by stacking a van der Waals ferromagnet Fe<sub>3</sub>GeTe<sub>2</sub> (FGT) on top of graphene to form an FGT/Gr heterostructure, we demonstrate a positive MR of up to ~9400% under a magnetic field of 9 T at room temperature (RT), an order of magnitude larger MR compared to pure graphene. More strikingly, the giant MR of the FGT/Gr heterostructure sustains over a wide temperature range from RT down to 4 K. Both control experiments and DFT calculations show that the enhanced MR originates from spin-dependent orbital coupling between FGT and graphene, which is temperature insensitive. Our results open a new route for realizing high-sensitivity and wide-temperature-range MR sensors.

MR is a fascinating magnetoelectric phenomenon that has attracted significant attention since decades ago due to its importance in both fundamental science and practical applications<sup>1–7</sup>. Researchers aim to develop MR sensors with low energy consumption and high sensitivity that can operate over a wide-temperature range. To achieve this, the MR of a variety of newcomer materials have been investigated in the past, including Dirac and Weyl semimetals<sup>8–13</sup>, strange metals<sup>14–16</sup>, etc. The most notable feature of these materials is the widespread unsaturated linear MR observed at cryogenic temperature. However, the MR usually maximizes at low temperature and decreases rapidly with increasing temperature<sup>9–13</sup>, which greatly limits their practical applicability. As a two-dimensional (2D) Dirac semimetal, graphene has been found to show unsaturated linear MR caused by spatial charge

inhomogeneity inevitably seen in 2D systems at room temperature<sup>17–21</sup>, holding great promise for future applications.

The MR of pristine graphene is finite, leaving a large room for improvement. According to the effective medium theory<sup>22</sup>, the degree of disorder or charge inhomogeneity in graphene directly affects its MR. Therefore, various methods have been proposed to enhance the MR of monolayer graphene by increasing its disorder. For example, different nanoparticles, such as gold<sup>23</sup>, cobalt<sup>24</sup> and nickel<sup>25</sup>, have been decorated on the surface of graphene. But, the enhancement of MR by such decoration method is not very effective. Alternative way to introduce extra disorder into graphene is to place it on exotic substrates such as lattice-mismatched black phosphorous<sup>26</sup>, surface-terraced SrTiO<sub>3</sub><sup>27</sup> and BiFeO<sub>3</sub> nano-island array<sup>28</sup>. By doing so, the

<sup>1</sup>Department of Physics, Engineering Research Center for Micro-Nano Optoelectronic Materials and Devices of Ministry of Education, Fujian Provincial Key Laboratory of Semiconductor Materials and Applications, Xiamen University, Xiamen, China. <sup>2</sup>National Institute for Materials Science, Tsukuba, Japan.

<sup>3</sup>Department of Physics, Southern University of Science and Technology, Shenzhen, China. <sup>4</sup>Shenzhen Institute for Quantum Science and Engineering, Southern University of Science and Technology, Shenzhen, China. <sup>5</sup>School of Optoelectronic Engineering and Instrumentation Science, Dalian University of Technology, Dalian, China. ✉e-mail: [fzhang@xmu.edu.cn](mailto:fzhang@xmu.edu.cn); [mywang@xmu.edu.cn](mailto:mywang@xmu.edu.cn); [dylfu@xmu.edu.cn](mailto:dylfu@xmu.edu.cn)

room-temperature MR has been enhanced significantly. However, the MR in these systems still shows severe temperature instability, which could be attributed to the highly temperature-dependent extrinsic degree of disorder. Very recently, Dirac plasma has been generated in graphene through sophisticated hexagonal boron nitride (h-BN) encapsulation technique, which achieves an MR as large as 110% under 0.1 T and 8600% under 9 T at room temperature<sup>29</sup>. However, the Dirac plasma only forms at the vicinity of Dirac point and sustains down to only -100 K, which makes the MR decrease dramatically at low temperature as well as away from Dirac point.

In order to achieve giant, stable MR in graphene in a broader temperature range, alternative strategy with temperature insensitivity needs to be introduced. Here, we propose a novel approach to enhance the MR of graphene by stacking the van der Waals ferromagnet FGT on a monolayer graphene to form an FGT/Gr heterostructure<sup>30,31</sup>. The FGT/Gr heterostructure can achieve a MR of up to -9400% under 9 T at room temperature away from Dirac point, which is more than thirty-fold enhancement over the MR of pure graphene. More importantly, the giant MR sustains in the full temperature range studied from RT down to 4 K and even slightly increases with lowering temperature. DFT calculations show that when FGT is placed on graphene, the magnetism of FGT breaks the spin-degeneracy of graphene, where the spin majority carriers with low mobility contribute little conductivity while the spin minority carriers

with high mobility dominates in transport. When an external magnetic field is applied, the density of spin minority carriers decreases rapidly, resulting in the reduction of conductivity and thus giant MR. Our work sheds light on the development of next generation MR sensors and relevant spintronic devices with high sensitivity and wide working-temperature range.

## Results and discussion

### Giant MR at room temperature

We fabricated the FGT/Gr heterostructure device by using a simple dry transfer method followed by standard electron-beam lithography and metal deposition procedure (see Methods for details). A typical device (Device A) is shown in Fig. 1a, where Hall-bar shaped electrodes are patterned directly on graphene ribbon, dividing the channel into two parts: pure graphene region and FGT/Gr heterostructure region. The MR for both regions were measured by recording the longitudinal resistance  $R_{xx}$  as a function of perpendicularly applied magnetic field  $B$  in a four-probe geometry and calculated as  $MR = (R_{xx}(B) - R_{xx}(0)) / R_{xx}(0) \times 100\%$ , where  $R_{xx}(B)$  and  $R_{xx}(0)$  are the resistance values at finite field and zero field, respectively.

The four-probe current-voltage ( $I$ - $V$ ) curves across the FGT/Gr heterostructure region under different magnetic fields were first measured and shown in Fig. 1b. As can be seen, the inverse slope of the  $I$ - $V$  curves, which corresponds to the longitudinal resistance  $R_{xx}$ ,

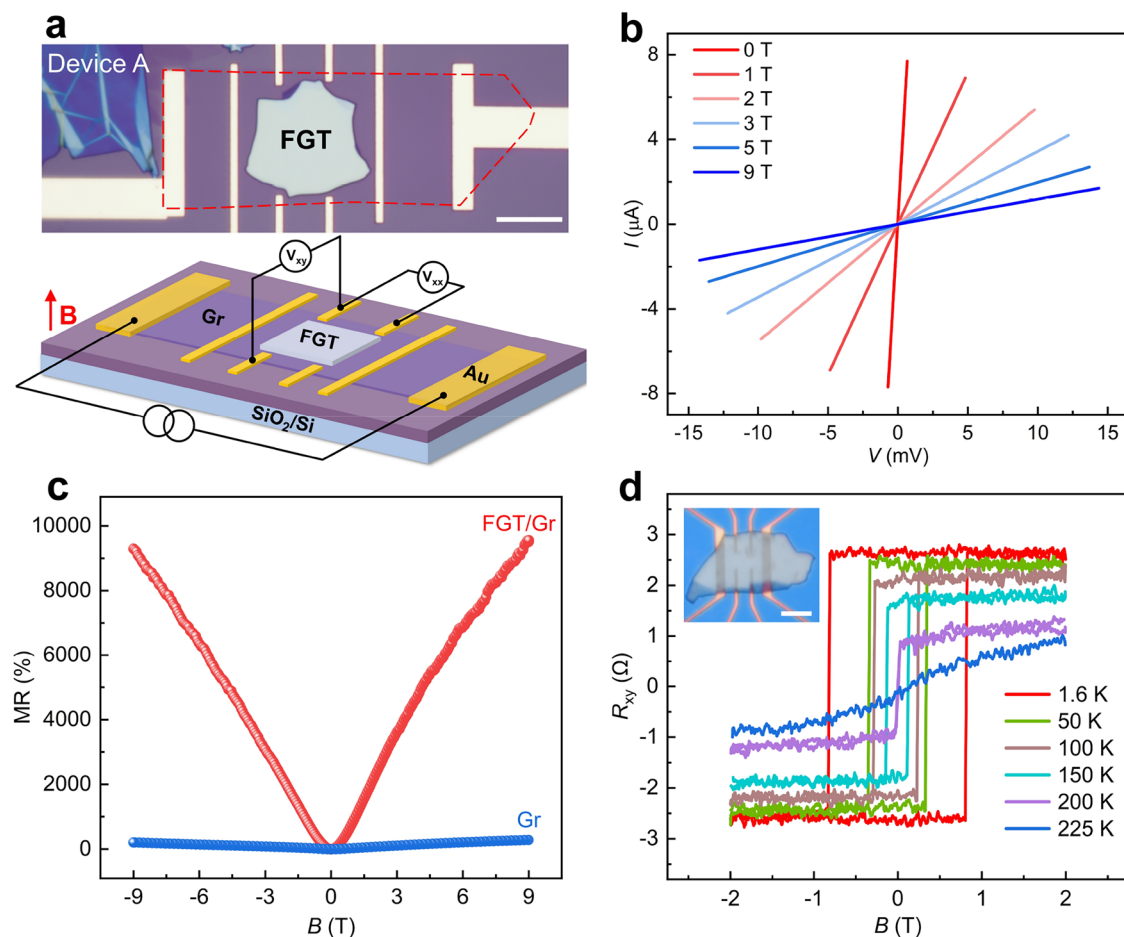


**Fig. 1 | Device structure and basic magneto-transport measurements at room temperature.** **a** Optical microscope image of a typical FGT/Gr heterostructure device (Device A) and schematic illustration of measurement setup. The red dashed line in the photograph indicates the monolayer graphene. Scale bar is 10  $\mu$ m. **b**  $I$ - $V$  curves of the FGT/Gr heterostructure in Device A under different magnetic fields.

**c** Room-temperature MR of the FGT/Gr heterostructure in Device A as a function of magnetic field. The MR curve of the pure graphene region is also shown for comparison. **d** Hall resistances  $R_{xy}$  of the FGT shown in the inset as a function of out-of-plane magnetic field at various temperatures ranging from 1.6 to 225 K. Scale bar is 5  $\mu$ m.

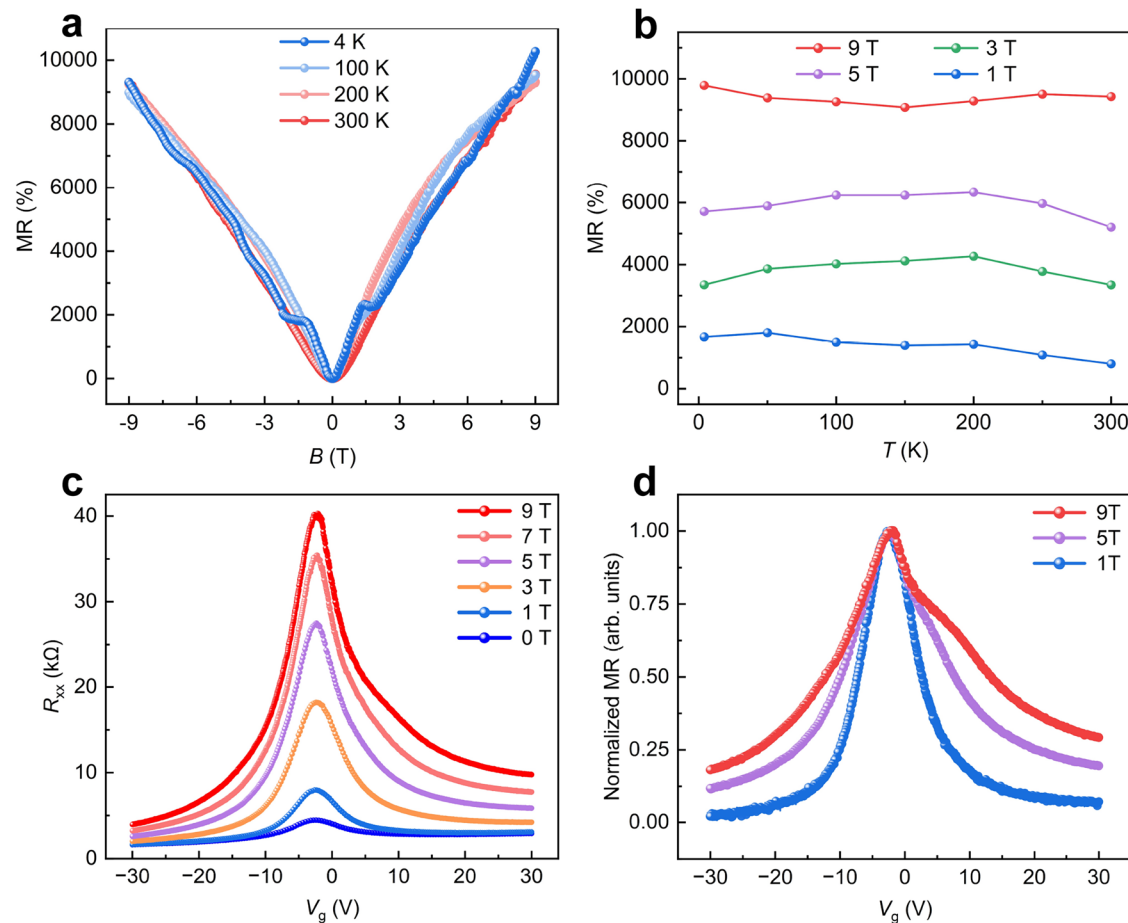


**Fig. 2 | Temperature- and gate-dependent MR of FGT/Gr heterostructure.** **a** The MR curves of FGT/Gr heterostructure in Device A as a function of magnetic field at different temperature points. **b** Variation of MR with temperature under different magnetic fields in Device A. **c** Transfer curves of FGT/Gr heterostructure in Device C

measured at room temperature under different magnetic fields. **d** Normalized MR of the FGT/Gr heterostructure in Device C under three representative magnetic fields as a function of gate voltage.

changes dramatically with increasing magnetic field, pointing to a large MR. Next, by scanning the magnetic field continuously under a constant sourcing current, the MR curves of both the graphene region and the FGT/Gr heterostructure region were measured, calculated and plotted in Fig. 1c. The MR of the FGT/Gr heterostructure reaches ~9400% under 9 T at room temperature, while that of the pure graphene is less than 300% which is comparable to previous reported values<sup>19,21</sup>. The more than thirty-fold enhancement of MR in our FGT/Gr heterostructure is appreciable and to the best of our knowledge, the absolute value sets a record as compared to previous reports on different graphene-based systems (refer to Fig. 4c and Supplementary Table 1)<sup>8,19–21,23–29</sup>.

The origin of the giant MR from FGT itself has to be ruled out first. The magneto-transport properties of FGT with comparable thickness (~40 nm) to that of the one used in Device A were characterized by making a Hall bar device as shown in the inset of Fig. 1d. The anomalous Hall effect measurement shows that the Curie temperature ( $T_c$ ) of the van der Waals ferromagnet FGT is ~210 K with an out-of-plane easy axis<sup>32</sup>. The MR curves of the FGT both below and above  $T_c$  were measured in the same way as aforementioned and shown in Supplementary Fig. 1. The negligibly small MR agrees with previous report<sup>33</sup>, indicating that the FGT alone cannot contribute to the giant MR observed in our FGT/Gr heterostructure.

### Temperature, angle and gate-dependence of MR

The MR curves at different temperatures in Device A were measured and shown in Fig. 2a. We note that the oscillatory and negative MR

usually seen at cryogenic temperature in pure graphene (Supplementary Fig. 5) and other graphene based heterostructures is absent in our system. Instead, the MR increases monotonically with magnetic field in the whole temperature range studied. These features suggest that the weak (anti)localization and universal conductance fluctuation are suppressed in our system<sup>26,27</sup>. The temperature-dependent MR under fixed magnetic fields were further plotted in Fig. 2b. Strikingly, the giant MR observed at room temperature stays almost unchanged when temperature decreases, in stark contrast to the trend observed in previously studied graphene-based systems<sup>8,19,20,23,26,29</sup>, which implies that the giant MR in our FGT/Gr heterostructure may have a different origin. We emphasize that such temperature-insensitive MR favors magnetic sensor applications at both room temperature and cryogenic temperature regimes. Next, the angular dependence of the  $R_{xx}$  on magnetic field direction was routinely checked and shown in Supplementary Figs. 2 and 5. The  $R_{xx}$  is at its maximum (minimum) when the magnetic field is perpendicular (parallel) to the sample surface, following a cosine dependence. Therefore, our FGT/Gr heterostructure complies with the classical MR mechanism, where the Lorentz force takes effect<sup>34</sup>.

Figure 2c shows the transfer curves of another device (Device C) under different magnetic fields. As can be seen, the Dirac point of graphene in the FGT/Gr heterostructure is at ~2.5 V under zero magnetic field and remains almost unchanged up to high magnetic fields. The gate-voltage-dependent MR was calculated from Fig. 2c and plotted in Fig. 2d for three representative magnetic fields. Similar to previous reports<sup>19,23,26,29</sup>, the MR is maximized around the Dirac point

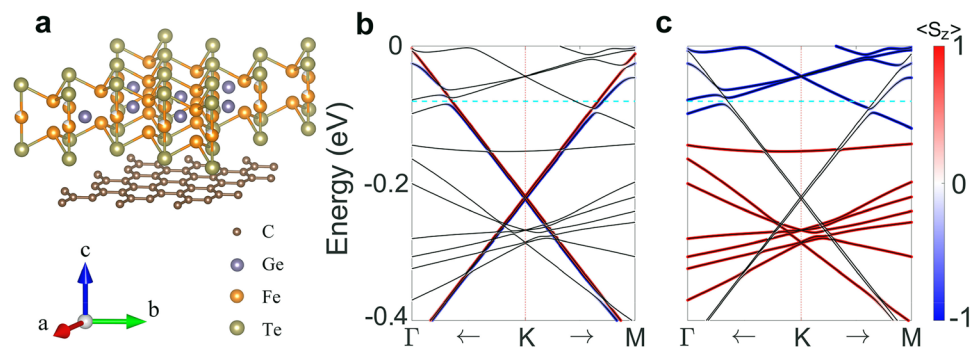


**Fig. 3 | Theoretical calculation.** **a** Crystal structure of FGT/Gr heterostructure. **b** The spin-resolution band structure, projected to graphene. **c** The spin-resolution band structure, projected to FGT. The dashed lines in both **(b, c)** indicate the Fermi level.

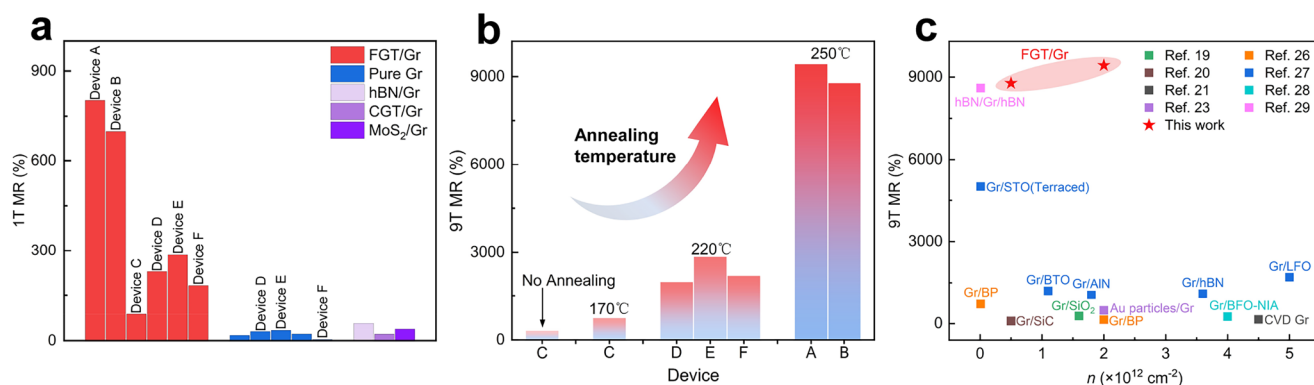


**Fig. 4 | Statistics of MR in different devices.** **a** Histogram of MR under 1 T magnetic field for different structures studied in this work. **b** Variation of MR under 9 T magnetic field with annealing temperature for different groups of devices. **c** Comparison of MR for different graphene-based systems reported in our work and literatures.

and decreases gradually away from it. It is noted that the MR decreases faster under low field while slower under high field.

### Understanding the origin of the giant MR

It is unclear why FGT, a ferromagnet with minimal MR on their own (less than 1% under 9 T), can increase the latter's MR by more than an order of magnitude when formed into heterostructures with monolayer graphene. To understand the physical mechanism inside, we performed a density functional theory (DFT)<sup>35,36</sup> calculation of FGT on monolayer graphene, as shown schematically in Fig. 3a. The spin resolution band structures projected to graphene and FGT are plotted in Fig. 3b, c, respectively. It can be seen from Fig. 3b that around Fermi energy (−0.08 eV), the spin-down bands (blue bands) of graphene are coupled with the spin-down bands of FGT, while the spin-up bands (red bands) of graphene almost keep its original linear dispersion, due to the lack of spin-up bands of FGT around the Fermi level, leading to strong hybridization of only one spin channel. Similar phenomenon has been reported in graphene proximitized by ferromagnetic insulator CrI<sub>3</sub> recently<sup>37</sup>. Here, we regard spin-down with larger density of states (DOS) at Fermi level as majority spin and spin-up with smaller DOS at Fermi level as minority spin. As well known, the high mobility of graphene originates from its linear dispersion and pseudo-spin of Dirac cone. Therefore, the breaking of the linear dispersion of graphene spin-down bands makes the majority spin carriers scattered by FGT easily, resulting in much lower mobility of majority spin carriers as compared with that of minority spin carriers. The total conductivity of graphene proximitized by FGT can be written as:  $\sigma_B = e(n_{\uparrow}\mu_{\uparrow} + n_{\downarrow}\mu_{\downarrow})$ , where  $n_{\uparrow/\downarrow}$  and  $\mu_{\uparrow/\downarrow}$  are the density and mobility of spin-up/down carriers, respectively. When there is no magnetic field, we have  $n_{\uparrow} < n_{\downarrow}$  and  $\mu_{\uparrow} \gg \mu_{\downarrow}$  as aforementioned, therefore the conductivity of graphene  $\sigma_{B=0} \approx en_{\uparrow}\mu_{\uparrow}$ . When an external magnetic field  $B$  is applied, the

spin-down bands move downward, with larger DOS, while the spin-up bands move upward, with smaller DOS. Based on conservation of particle number,  $n_{\uparrow} + n_{\downarrow} + N_{\text{FGT},\downarrow} = \text{Const.}$ , we have  $\delta n_{\uparrow} = \delta n_{\downarrow} + \delta N_{\text{FGT},\downarrow}$  ( $\delta n \equiv |n(B) - n(B=0)|$ ), which means that the density of spin-up (minority) carriers  $n_{\uparrow}$  reduces much faster than spin-down (majority) carriers  $n_{\downarrow}$  increases, resulting in rapid reduction of the conductivity of graphene  $\sigma_B \approx en_{\uparrow}(B)\mu_{\uparrow}$  and therefore the giant MR.

To demonstrate the uniqueness of FGT on the enhancement of the MR in graphene, we stacked CrGeTe<sub>3</sub> (CGT)<sup>38</sup>, a 2D ferromagnetic semiconductor, on monolayer graphene to make a CGT/Gr heterostructure device. The device image and measurement results are presented in Supplementary Fig. 8. It is found that there is no MR enhancement at all and the MR of the heterostructure even decreases as compared to the pure graphene. DFT calculations on the CGT/Gr heterostructure were also performed and the results are shown in Supplementary Fig. 9. Different from the FGT/Gr case, the energy band hybridization between CGT and graphene is inappreciable, therefore spin-dependant orbital coupling induced MR enhancement effect is not expected as shown in Supplementary Fig. 8. Likewise, we also stacked MoS<sub>2</sub>, a 2D nonmagnetic semiconductor, with monolayer graphene to make a MoS<sub>2</sub>/Gr heterostructure device. The measurement results presented in Supplementary Fig. 10 also show negligible MR enhancement effect. The MR obtained from different heterostructures in our work are summarized in Fig. 4a, where only FGT/Gr shows giant MR as compared to others, pointing to the unique role of FGT on enhancing the MR in graphene as aforementioned.

We also note that vacuum annealing can help to improve the coupling between FGT and graphene, therefore enhance the MR of the heterostructure. It is a common way to do vacuum annealing in order to enhance the interfacial coupling in van der Waals heterostructures

by driving out the trapped air/moisture as much as possible<sup>39–42</sup>, which depends on the annealing temperature and time. As shown in Fig. 4b and Supplementary Fig. 4c, the as-fabricated FGT/Gr heterostructure shows MR of only ~300% under 9 T (Device C), which is nevertheless still higher than that of pure graphene. After annealing in high vacuum at 170 °C (see Methods), the MR of the heterostructure drastically increased to ~760%. For devices with even higher annealing temperature (220 °C and 250 °C), the MR all reached above ~2000% with highest value of ~9400%. For pure graphene and other heterostructures studied in this work, however, vacuum annealing showed little enhancement of the MR. This further supports that the giant MR in FGT/Gr heterostructure originates from the unique interfacial coupling induced spin-split band hybridization between FGT and graphene, rather than other artificial effects.

In summary, giant MR of up to ~9400% under 9 T at room temperature has been observed in FGT/Gr heterostructure, in which the more than one order of magnitude enhancement of MR as compared to pure graphene originates from spin-dependent orbital coupling between FGT and graphene. While in graphene heterostructures formed with either ferromagnetic semiconductor CGT or non-ferromagnetic semiconductor MoS<sub>2</sub>, such spin-dependent coupling is negligible, leading to little MR enhancement. Strong spin-dependent hybridization was recently predicted in CrI<sub>3</sub>/Gr heterostructure<sup>37</sup>, therefore similar MR enhancement effect may also exist, which needs to be further studied. More importantly, the giant MR of FGT/Gr heterostructure at room temperature stays almost unchanged with decreasing temperature, which is strikingly different from the temperature-dependent behavior in previously reported systems. With rapid advancement of growing large-area graphene and related 2D materials, our work holds an attractive prospect for fabricating highly sensitive graphene-based magnetic sensors with wide temperature operation ranges.

## Methods

### Heterostructure preparation and device fabrication

Monolayer graphene was prepared by mechanically peeling high-quality graphite (natural graphite from HQ Graphene) onto SiO<sub>2</sub>(285 nm)/Si substrate and identified by optical contrast as well as Raman spectra. Multilayer Fe<sub>3</sub>GeTe<sub>2</sub> was exfoliated and transferred onto monolayer graphene by PDMS dry transfer technique in glove box (O<sub>2</sub>, H<sub>2</sub>O < 1 ppm). Electrodes were patterned by e-beam lithography and then Ti/Au (2 nm/50 nm) was deposited by an e-beam evaporator with base pressure of 10<sup>-7</sup> Torr. Standard lift-off procedure was done subsequently and blowed dry with Ar gun. Finally, multilayer h-BN was exfoliated and transferred onto the device channel region to prevent Fe<sub>3</sub>GeTe<sub>2</sub> from being oxidized in air. For CGT/Gr and MoS<sub>2</sub>/Gr heterostructure devices, same procedures were followed. For vacuum annealing, device was put into a tube furnace equipped with turbo pump station (base pressure: 10<sup>-6</sup> Torr) and kept at different temperatures for 3 h.

### Magneto-transport measurements

The magneto-transport measurements were carried out in a Cryofree superconducting magnet system (CFMS-12T-30VTI, Cryogenic Co.) with magnetic field up to 12 T by using two source meters (Model 2400 and Model 2450, Keithley Inc.). To apply back gate voltage, the source terminal was connected to the back gate and the leakage current through the SiO<sub>2</sub> dielectric layer was monitored.

### Theoretical calculation details

The first-principles calculations were performed using Vienna ab initio simulation package (VASP) based on the density function theory with LDA + U. The energy cut off of the plane wave basis was set as 400 eV, and the Brillouin zone was sampled by 6 × 6 × 1 k-mesh.

## Data availability

The source data generated in this study have been deposited in the *figshare* database under accession code<sup>43</sup>.

## References

- Baibich, M. N. et al. Giant magnetoresistance of (001)Fe/(001)Cr magnetic superlattices. *Phys. Rev. Lett.* **61**, 2472–2475 (1988).
- Abrikosov, A. A. Quantum linear magnetoresistance. *Europhys. Lett.* **49**, 789–793 (2000).
- Parish, M. M. & Littlewood, P. B. Non-saturating magnetoresistance in heavily disordered semiconductors. *Nature* **426**, 162–165 (2003).
- Parkin, S. S. P. et al. Giant tunnelling magnetoresistance at room temperature with MgO (100) tunnel barriers. *Nat. Mater.* **3**, 862–867 (2004).
- Ripka, P. & Janosek, M. Advances in magnetic field sensors. *IEEE Sens. J.* **10**, 1108–1116 (2010).
- Friedman, A. L. et al. Quantum linear magnetoresistance in multi-layer epitaxial graphene. *Nano Lett.* **10**, 3962–3965 (2010).
- Fang, J. Z. et al. Large unsaturated magnetoresistance of 2D magnetic semiconductor Fe-SnS<sub>2</sub> homojunction. *J. Semicond.* **43**, 092501 (2022).
- Cho, S. & Fuhrer, M. S. Charge transport and inhomogeneity near the minimum conductivity point in graphene. *Phys. Rev. B* **77**, 081402(R) (2008).
- Ali, M. N. et al. Large, non-saturating magnetoresistance in WTe<sub>2</sub>. *Nature* **514**, 205–208 (2014).
- Liang, T. et al. Ultrahigh mobility and giant magnetoresistance in the Dirac semimetal Cd<sub>3</sub>As<sub>2</sub>. *Nat. Mater.* **14**, 280–284 (2015).
- Thoutam, L. R. et al. Temperature-dependent three-dimensional anisotropy of the magnetoresistance in WTe<sub>2</sub>. *Phys. Rev. Lett.* **115**, 046602 (2015).
- Shekhar, C. et al. Extremely large magnetoresistance and ultrahigh mobility in the topological Weyl semimetal candidate NbP. *Nat. Phys.* **11**, 645–649 (2015).
- Kumar, N. et al. Extremely high magnetoresistance and conductivity in the type-II Weyl semimetals WP<sub>2</sub> and MoP<sub>2</sub>. *Nat. Commun.* **8**, 1642 (2017).
- Phillips, P. W., Hussey, N. E. & Abbamonte, P. Stranger than metals. *Science* **377**, eabh4273 (2022).
- Hayes, I. et al. Scaling between magnetic field and temperature in the high-temperature superconductor BaFe<sub>2</sub>(As<sub>1-x</sub>P<sub>x</sub>)<sub>2</sub>. *Nat. Phys.* **12**, 916–919 (2016).
- Giraldo-Gallo, P. et al. Scale-invariant magnetoresistance in a cuprate superconductor. *Science* **361**, 479–481 (2018).
- Novoselov, K. S. et al. Two-dimensional gas of massless Dirac fermions in graphene. *Nature* **438**, 197–200 (2005).
- Castro Neto, A. H., Guinea, F., Peres, N. M. R., Novoselov, K. S. & Geim, A. K. The electronic properties of graphene. *Rev. Mod. Phys.* **81**, 109–162 (2009).
- Gopinadhan, K., Shin, Y. J., Yudhistira, I., Niu, J. & Yang, Y. Giant magnetoresistance in single-layer graphene flakes with a gate-voltage-tunable weak localization. *Phys. Rev. B* **88**, 195429 (2013).
- Chuang, C. S., Yang, Y. F., Elmquist, R. E. & Liang, C.-T. Linear magnetoresistance in monolayer epitaxial graphene grown on SiC. *Mater. Lett.* **174**, 118–121 (2016).
- Chuang, C. S. et al. Large, non-saturating magnetoresistance in single layer chemical vapor deposition graphene with an h-BN capping layer. *Carbon* **136**, 211–216 (2018).
- Tiwari, R. P. & Stroud, D. Model for the magnetoresistance and Hall coefficient of inhomogeneous graphene. *Phys. Rev. B* **79**, 165408 (2009).
- Jia, Z. Z. et al. Large tunable linear magnetoresistance in gold nanoparticle decorated graphene. *Appl. Phys. Lett.* **105**, 143103 (2014).

24. Wang, Q. et al. Enhanced room-temperature positive magnetoresistance of graphene by decorating Co particles on the surface. *Mater. Lett.* **293**, 129730 (2021).
25. Cruz, E. A., Ducos, P., Gao, Z., Johnson, A. T. C. & Niebieskikwiat, T. Exchange coupling effects on the magnetotransport properties of Ni-nanoparticle-decorated graphene. *Nanomaterials* **13**, 1861 (2023).
26. Liu, Y. P. et al. Phonon-mediated colossal magnetoresistance in graphene/black phosphorus heterostructures. *Nano Lett.* **18**, 3377 (2018).
27. Hu, J. X. et al. Room-temperature colossal magnetoresistance in terraced single-layer graphene. *Adv. Mater.* **32**, 2002201 (2020).
28. Jeon, J. et al. Large temperature-independent magnetoresistance without gating operation in monolayer graphene. *ACS Appl. Mater. Interfaces* **12**, 53134 (2020).
29. Xin, N. et al. Giant magnetoresistance of Dirac plasma in high-mobility graphene. *Nature* **616**, 270–274 (2023).
30. Deng, Y. et al. Gate-tunable room-temperature ferromagnetism in two-dimensional  $\text{Fe}_3\text{GeTe}_2$ . *Nature* **563**, 94–99 (2018).
31. Gibertini, M., Koperski, M., Morpurgo, A. F. & Novoselov, K. S. Magnetic 2D materials and heterostructures. *Nat. Nanotechnol.* **14**, 408–419 (2019).
32. Feng, H. et al. Resistance anomaly and linear magnetoresistance in thin flakes of itinerant ferromagnet  $\text{Fe}_3\text{GeTe}_2$ . *Chin. Phys. Lett.* **39**, 077501 (2022).
33. Zeng, X. et al. Magnetoresistance studies of two-dimensional  $\text{Fe}_3\text{GeTe}_2$  nano-flake. *J. Phys.: Condens. Matter* **34**, 345701 (2022).
34. Gopinadhan, K. et al. Extremely large magnetoresistance in few-layer graphene/boron–nitride heterostructures. *Nat. Commun.* **6**, 8337 (2015).
35. Kresse, G. & Furthmüller, J. Efficient iterative schemes for ab initio total-energy calculations using a plane-wave basis set. *Phys. Rev. B* **54**, 11169 (1996).
36. Kresse, G. & Joubert, D. From ultrasoft pseudopotentials to the projector augmented-wave method. *Phys. Rev. B* **59**, 1758–1775 (1999).
37. Cardoso, C., Costa, A. T., MacDonald, A. H. & Fernández-Rossier, J. Strong magnetic proximity effect in van der Waals heterostructures driven by direct hybridization. *Phys. Rev. B* **108**, 184423 (2023).
38. Li, X. X. & Yang, J. L.  $\text{CrXTe}_3$  (X = Si, Ge) nanosheets: two dimensional intrinsic ferromagnetic semiconductors. *J. Mater. Chem. C* **2**, 7071–7076 (2014).
39. Diaz, H. C., Addou, R. & Batzill, M. Interface properties of CVD grown graphene transferred onto  $\text{MoS}_2$ (0001). *Nanoscale* **6**, 1071–1078 (2014).
40. Wang, K. et al. Interlayer coupling in twisted  $\text{WSe}_2/\text{WS}_2$  bilayer heterostructures revealed by optical spectroscopy. *ACS Nano* **10**, 6612–6622 (2016).
41. Yue, X. et al. Monitoring and engineering interface coupling between monolayer  $\text{WS}_2$  and substrate through controllably introducing interfacial strain. *Sci. China Mater.* **67**, 3012–3020 (2024).
42. Tang, L. et al. Enhancing magnetocrystalline anisotropy through interface coupling in a 2D ferromagnetic  $\text{Fe}_3\text{GeTe}_2/\text{VI}_3$  heterostructure. *Appl. Phys. Lett.* **124**, 012403 (2024).
43. Huang, S. et al. Giant magnetoresistance induced by spin-dependent orbital coupling in  $\text{Fe}_3\text{GeTe}_2$ /graphene heterostructures. *figshare*. Dataset. <https://doi.org/10.6084/m9.figshare.28539461> (2025).
- Central Universities (No. ZK1245). M.W. acknowledges support by the Natural Science Foundation of Xiamen, China (No. 35022202472008). F.Z. acknowledges support by the National Natural Science Foundation of China (Nos. 62274137 and 62104222), Natural Science Foundation of Jiangxi Province of China for Distinguished Young Scholars (No. S2021QNZD2L0013) and National Key Research and Development Program of China (No. 2023YFB3609500). J.X., L.W. and J.M. acknowledge support by the National Key Research and Development Program of China (No. 2021YFA1400400) and the Shenzhen Fundamental Research Program (Nos. JCYJ20220818100405013 and JCYJ20230807093204010). H.H. acknowledges support by the Science and Technology Innovation Fund of Dalian (No. 2022JJ12GX011).

## Author contributions

D.F. and R.Z. initiated, coordinated, and supervised the work. S.H., L.Z. and Y.Z. fabricated the devices. S.H. performed the measurements. M.W. did the theoretical calculations. J.X., L.W. and J.M. grew the  $\text{Fe}_3\text{GeTe}_2$  crystals. K.W. and T.T. grew the h-BN crystals. S.H., F.Z., M.W. and D.F. participated in the data analysis and manuscript writing.

## Competing interests

The authors declare no competing interests.

## Additional information

**Supplementary information** The online version contains supplementary material available at <https://doi.org/10.1038/s41467-025-58224-4>.

**Correspondence** and requests for materials should be addressed to Feng Zhang, Maoyuan Wang or Deyi Fu.

**Peer review information** *Nature Communications* thanks Jung-Woo Yoo and the other, anonymous, reviewer(s) for their contribution to the peer review of this work. A peer review file is available.

**Reprints and permissions information** is available at <http://www.nature.com/reprints>

**Publisher's note** Springer Nature remains neutral with regard to jurisdictional claims in published maps and institutional affiliations.

**Open Access** This article is licensed under a Creative Commons Attribution-NonCommercial-NoDerivatives 4.0 International License, which permits any non-commercial use, sharing, distribution and reproduction in any medium or format, as long as you give appropriate credit to the original author(s) and the source, provide a link to the Creative Commons licence, and indicate if you modified the licensed material. You do not have permission under this licence to share adapted material derived from this article or parts of it. The images or other third party material in this article are included in the article's Creative Commons licence, unless indicated otherwise in a credit line to the material. If material is not included in the article's Creative Commons licence and your intended use is not permitted by statutory regulation or exceeds the permitted use, you will need to obtain permission directly from the copyright holder. To view a copy of this licence, visit <http://creativecommons.org/licenses/by-nc-nd/4.0/>.

© The Author(s) 2025

## Acknowledgements

D.F. acknowledges support by the National Natural Science Foundation of China (No. 62174143) and the Fundamental Research Funds for the